Orientation of Cobalt-Phthalocyanines on Molybdenum Disulfide: Distinguishing between Single Crystals and Small Flakes

Philipp Haizmann,[#] Eric Juriatti,[#] Maren Klein, Katharina Greulich, Peter Nagel, Michael Merz, Stefan Schuppler, Amir Ghiami, Ruslan Ovsyannikov, Erika Giangrisostomi, Thomas Chassé, Marcus Scheele,[*] and Heiko Peisert[*]

ABSTRACT: Heterostructures consisting of transition metal dichalcogenides (TMDCs) and organic molecules are currently of enormous interest for a variety of applications. Comparably weakly interacting molecules, like phthalocyanines, exhibit a high potential for tuning the electronic properties of TMDCs. Knowledge of the molecular orientation is a prerequisite for understanding the nature and strength of the interfacial interaction. We study the molecular orientation of cobalt phthalocyanine (CoPc) and perfluorinated cobalt phthalocyanine ($CoPcF_{16}$, also denoted $F_{16}CoPc$), on both large molybdenum disulfide (MoS_2) single crystals and small MoS_2 flakes, using synchrotron-based techniques: X-ray absorption spectroscopy (XAS) at the Co L_3 edge and spectromicroscopy in a photoemission electron microscope (PEEM). We show that the orientation can be radically different on both substrates. Whereas on large crystals an almost flat-lying orientation is observed, significant tilt angles were found on smaller flakes. It is proposed that the orientation depends crucially on the number of MoS_2 layers and/or the smaller size of atomically flat terraces on flakes compared to bulk crystals.

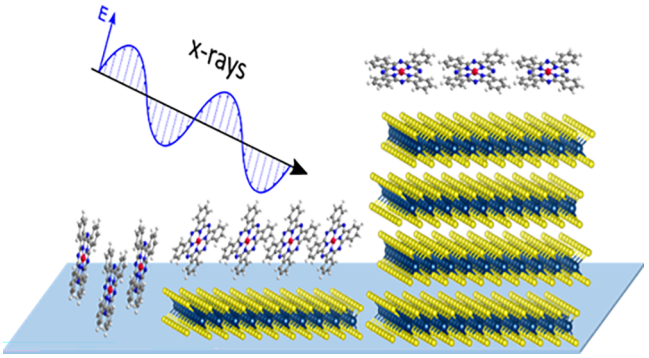

1. INTRODUCTION

Due to their remarkable physical and chemical properties, layered transition metal dichalcogenides (TMDCs) are a promising class of materials for future applications in modern semiconductor devices for electronics, lighting, solar energy, and communication. In particular, it is expected that these materials will enable the further miniaturization of electronic devices according to Moore's law[1,2] and promote the establishment of flexible electronic devices.[3] The layered structure allows for exfoliation down to 2D layers with unique electronic properties compared to their bulk counterparts; in the case of MoS_2, the nature of the band gap changes from direct to indirect.[4−6] Especially, TMDC monolayers and heterostructures are of interest for a broad variety of devices.[2,7−9]

One approach for tuning the electronic properties is the formation of TMDC/organic semiconductor heterostructures. Recent research on conjugated organic molecule/TMDC interfaces has been mainly focused on strong molecular electron acceptors.[10−13] However, weaker interacting, physisorbed organic molecules may also interact with TMDCs. Such systems are expected to offer new opportunities for tuning both optical and electronic characteristics.[14] For example, a quenching of the low-temperature defect photoluminescence of MoS_2 was observed after the adsorption of metal-phthalocyanines, depending strongly on the central metal atom of the phthalocyanine.[15] The nature of such interactions is currently being increasingly discussed,[16] and one crucial parameter in this regard is the orientation of the molecules with respect to the substrate surface. For example, the coupling between nickel phthalocyanine (NiPc) and graphene is supported by the flat geometry of the NiPc complexes.[17] Especially for anisotropic organic semiconductor films, the orientation of the individual molecules at the heterostructure is of particular significance, since it influences the electronic properties of the film and, therefore the overall interaction at the interface.[18,19]

We study the molecular orientation of cobalt phthalocyanine (CoPc) and perfluorinated cobalt phthalocyanine ($CoPcF_{16}$) on MoS_2 bulk crystals and on exfoliated pieces, often called flakes, which have fewer and even monolayer thickness—a system, where weak interactions at interfaces (i.e., the absence of an integer charge transfer) can be expected. Representatives

of the family of transition metal phthalocyanines (TMPcs) were chosen due to their advantageous chemical and physical properties, including stability, film growth, and tunability of electronic parameters due to the variation of the central metal and the selection of the peripheral substituents.[20−23] Fluorination of the Pc moiety increases the ionization energy by more than 1 eV,[24−27] which may significantly affect electronic interactions at interfaces, even in the case of metal surfaces passivated by graphene.[28] Numerous studies on the growth of phthalocyanines were carried out on a broad variety of substrates. On single-crystalline substrates, the almost planar phthalocyanine molecules typically prefer a predominantly flat-lying orientation (see, e.g., refs 20, 29−35); this includes also van der Waals substrates like GeS or MoS_2, and graphene-covered metal substrates.[30,32−35] In contrast, on polycrystalline substrates, the molecular orientation can be radically different, depending crucially on the substrate roughness.[29,30] The different growth modes observed on various substrates can be understood in terms of different molecule−substrate and molecule−molecule interactions at the interface.[29,36−38] In conclusion, higher tilt-angles for phthalocyanines on single crystals were in particular found if the molecule−substrate interaction is weaker, e.g., for van-der-Waals solids or passivated semiconductor surfaces.[32,39]

In this study, we demonstrate that the orientations of CoPc and $CoPcF_{16}$ on molybdenum disulfide flakes can diverge from that on the bulk MoS_2 single crystal. Therefore, the prediction of the molecular orientation on thin flakes from literature data obtained with bulk crystals only could be misleading for differing structural situations.

2. METHODS

Cobalt phthalocyanine (CoPc, Sigma-Aldrich Chemie GmbH) and perfluorinated cobalt phthalocyanine ($CoPcF_{16}$, Sigma-Aldrich Chemie GmbH) were deposited on synthetic bulk 2H-phase MoS_2 (2D Semiconductors Inc. USA) by thermal evaporation under ultrahigh vacuum (UHV) conditions (base pressure about 1×10^{-9} mbar). The evaporation chamber was directly attached to the spectrometer chamber. The nominal film thickness was determined using a quartz crystal microbalance (QCM), setting the mass density of CoPc and $CoPcF_{16}$ at 1.6 g/cm^3 and 2.0 g/cm^3, respectively,[40,41] and checked by the comparison of X-ray photoelectron spectroscopy (XPS) peak areas for bulk MoS_2 sample experiments.

For the studies of bulk MoS_2, the crystals were cleaved by adhesive tape in UHV. No further annealing was performed. The cleanliness was checked by XPS. These experiments were conducted at the PM4 beamline of the BESSY II electron storage ring operated by the Helmholtz-Zentrum Berlin (HZB) using the LowDosePES endstation.[42] Polarization-dependent X-ray absorption spectroscopy (XAS) measurements at the N K and Co L edges were carried out in total electron yield mode, measuring the sample drain current and orienting the sample at different polar angles with respect to the incoming beam of fixed horizontal polarization. The correction for beamline characteristics of the photon flux was carried out using the drain current from the last beamline mirror or XAS spectra of pristine gold substrates. The XAS spectra were normalized to the same step height, well above the absorption edge.

For determining the orientation of CoPc and $CoPcF_{16}$ on MoS_2 flakes, laterally resolved spectromicroscopy experiments in a photoemission electron microscope (PEEM) were conducted at the Institute for Quantum Materials and Technologies soft X-ray beamline WERA at the KIT Light Source, Karlsruhe, Germany. The degree of linear polarization was set to nominal values between 72 and 93%, all giving sufficient orientational contrast of the Co L edge with photon energies between 770 eV − 800 eV. The energy resolution was set to 490 meV. The PEEM (FOCUS GmbH) has an integrated sample stage (IS), an imaging energy filter (IEF) using a retarding field, and operates in a fixed geometry; the angle between the p-polarized incident photon beam and the normal of the sample was 65°. Since the fixed geometry does not allow a direct determination of the molecular orientation, the adsorption geometry was estimated from the known angular dependence of polarization dependent XAS spectra (measured, for example, on bulk MoS_2). Flat and dark field corrections were considered in the postprocessing of the measured image stacks. The incident photon flux was monitored by using a clean gold mesh.

Ultraviolet photoelectron spectroscopy (UPS) measurements at our laboratory spectrometer were performed inside a multichamber UHV system (base pressure of 1×10^{-9} mbar) equipped with an ultraviolet source (UVS 300, Specs) and a Phoibos 150 hemispherical photoelectron analyzer (Specs). The energy calibration was performed by using argon-sputtered and annealed Ag foils at the Fermi edge. The energy resolution was 150 meV.

MoS_2 flakes, containing regions with varying numbers of layers, were prepared *ex-situ* for PEEM measurements using the top-down scotch tape method, starting with synthetic bulk MoS_2 (2D Semiconductors Inc., USA).[43] Since MoS_2 crystals used for both exfoliation and experiments on bulk MoS_2 were purchased from the same company, we assume a similar quality of MoS_2 layers for both types of experiments. Exfoliated flakes were transferred onto a polydimethylsiloxane stamp (PF Gel Film, Teltec GmbH). The stamp is pressed onto the substrates, leaving thin-layers of TMDC on them. As substrates, we used commercially available silicon wafers. Part of the silicon wafers were coated with 50 nm of titanium at an evaporation rate of 0.1 nm/s, determined by QCM, and used after exposure to environmental conditions as a substrate for the transfer of the flakes. The XPS analysis reveals that the native oxide covers the surface completely; no metallic Ti was detectable. To fit the dimensions of the PEEM sample holders, 7.5 mm × 7.5 mm substrates were cut from these wafers. Native titanium oxide and silicon oxide layers were found on both surfaces, as evidenced by photoemission measurements (Figures S1−S3, Supporting Information). The substrates were ultrasonically cleaned with a solvent cascade, starting with acetone followed by hexane, ethyl acetate, and isopropanol. As a final cleaning step, the substrates were placed in a UV oven (Photo Surface Processor PL16−110B-1, Sen Lights Corp) for 15 min. Successful transfers of the MoS_2 flakes were evaluated by optical microscope images. Those images were taken with an Olympus BHM microscope equipped with an EOS600D camera (Canon) and a NeoDPlan 50 (Olympus) objective. As this preparation method yields a large number of flakes with different thicknesses on the substrates, we selected the most promising ones based on contrast assessments. The images of the flakes selected for later experiments are shown in Figure 2a−c. Prior to the deposition of phthalocyanines, the samples were annealed under UHV conditions to 250 °C for 12 h to remove contamination from preparation and ensure a clean

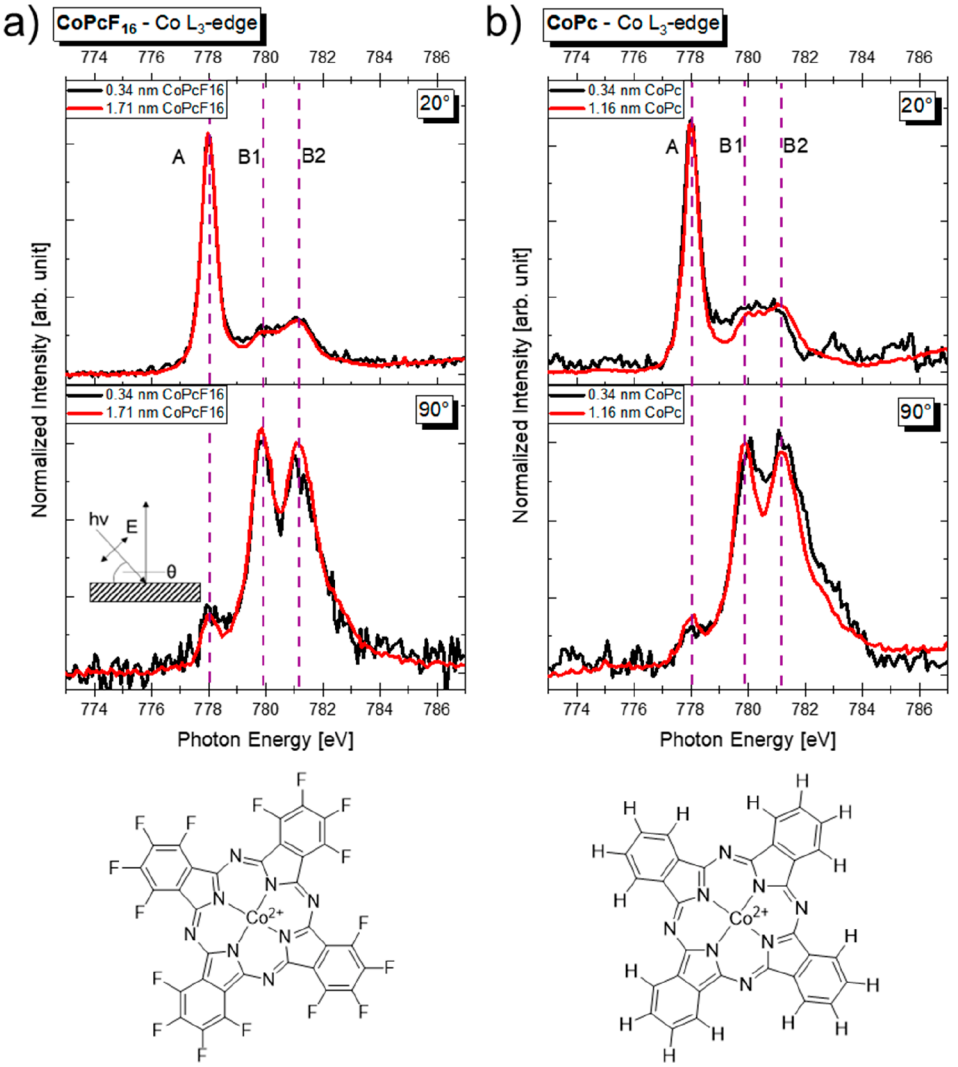

Figure 1. Angle-dependent XAS measurements in the Co L_3 region show intensity differences of features A and the two B features depending on the orientation of the electric field with respect to the sample for $CoPcF_{16}$ shown in (a) and CoPc shown in (b) on bulk MoS_2, with the respective structural formula below each spectrum.

surface, as verified by PEEM measurements (see Figure S1–S3).

For the evaluation of the PEEM results and optical microscopy images, we used the software ImageJ/Fiji[44,45] with the plugin FeatureJ from Erik Meijering.

3. RESULTS AND DISCUSSION

Polarization-dependent X-ray absorption spectroscopy (XAS) offers an optimal method for studying the adsorption geometry of molecular adsorbates.[29,46] For the planar TMPcs having D_{4h} symmetry, both C 1s–π^* or N 1s–π^* excitations are suitable for determining molecular orientation.[29] If the electric field vector of the incoming light is oriented parallel to the atomic p_z wave functions forming the molecular π^* orbital (i.e., out of the molecular plane), then the absorption is maximal. In contrast, the transition is forbidden in the case of a perpendicular orientation.[46,47] However, in our case, the analysis of the N K edge absorption spectra is hindered by the overlap with features from the MoS_2 substrate. An example of a N K edge spectrum of a $CoPcF_{16}$ monolayer in superposition with Mo $M_{3,2}$, is shown in Figure S4a (Supporting Information) and for a thicker $CoPcF_{16}$ film in Figure S4b. Also, the analysis of the C K edge is very difficult due to common carbon contaminations of beamline components and residual carbon in *ex situ* prepared samples, especially for monolayer coverages. However, Co L edge XAS spectra also show a pronounced angular dependence (see, e.g., refs 34 and 48). They are determined to a large extent by multiplet effects due to the strong overlap between core level and valence wave functions.[49] Nevertheless, in-plane and out-of-plane transitions can be distinguished (for details, we refer to the literature, e.g. refs 50 and 51). In the following, we use the shape of the Co L_3 XAS spectra for the estimation of the molecular orientation. We note that the shape of these spectra is almost independent of the fluorination of CoPc (see, e.g., refs 34 and 52).

In Figure 1, polarization-dependent Co L_3 edge spectra of (Figure 1a) $CoPcF_{16}$ and (Figure 1b) CoPc on bulk MoS_2 are shown for two different film thicknesses measured at two different incidence angles of the p-polarized light. Transitions polarized perpendicular to the molecular plane (z-polarized) are denoted A, whereas B features are polarized within the molecular plane (xy-polarized). Consistent with the considerations above, the intensity of the out-of-plane feature A is

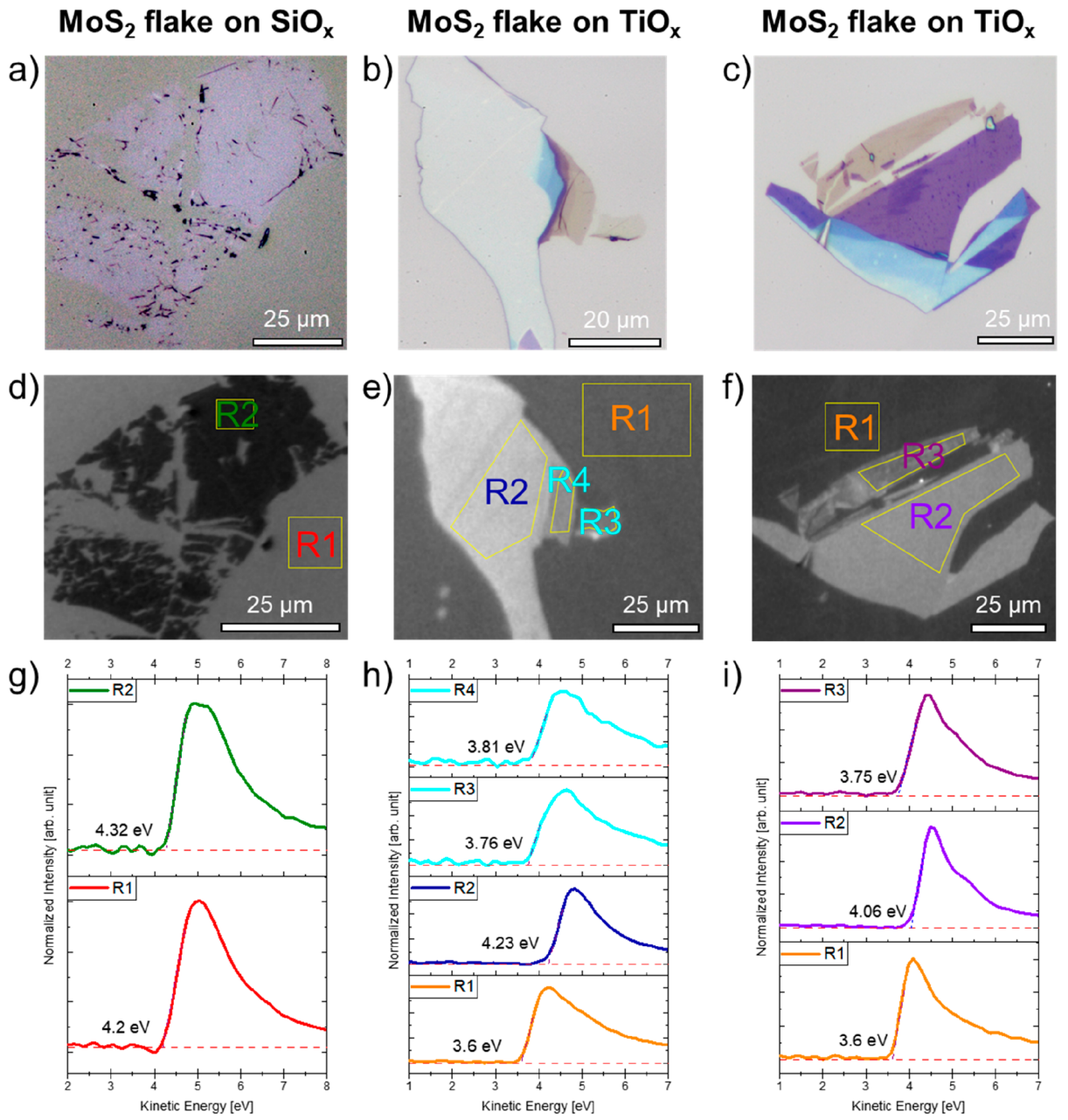

Figure 2. (a–c) Optical microscope images of MoS_2 flakes on SiO_x (a, flake 1) and on TiO_x substrates (b) and (c), flake 2 and flake 3 respectively. Averaged images of the work function contrast sequence for the samples containing flake 1, flake 2 and flake 3 are shown in (d), (e) and (f) respectively. The grayscale is arbitrary to maximize contrast. (g–i) μ-PES spectra of the secondary electron cutoff and the calculated work functions.

maximal close to grazing incidence (20°), whereas the in-plane transitions B are most intense at normal incidence (90°). This indicates a preferred orientation of the molecule parallel to the substrate surface (referred to as face-on). The spectral shape of the Co L_3 edge is almost identical for the coverage in the monolayer range (0.34 nm) and in the multilayer film, indicating that the orientation of the first molecular layer is maintained in the thin film. This behavior on bulk MoS_2 substrates is identical for CoPc and $CoPcF_{16}$. A more detailed comparison of the spectral shapes in Figure 1 with literature data (e.g., refs.[34,48,52]) reveals that tilt angles between the molecules and the substrate surface are rather small or even negligible. Thus, we can conclude that an orientation close to a face-on configuration of CoPc and $CoPcF_{16}$ is favored on bulk MoS_2.

The observed predominant face-on alignment of cobalt phthalocyanines is in good agreement with related systems, such as the previously studied $FePc(F_x)$ molecules on MoS_2.[33] However, it is essential to recognize that this orientation could be influenced by numerous factors on more frequently studied MoS_2 samples, like 2D layers or flakes. For instance, the roughness of the substrate surface and the size of its atomically flat terraces can significantly impact the alignment of molecules.[29] This leads to the question of whether the determined molecular orientation of cobalt phthalocyanines on bulk MoS_2 applies also to smaller MoS_2 flakes, which are of particular interest for applications. Due to the small

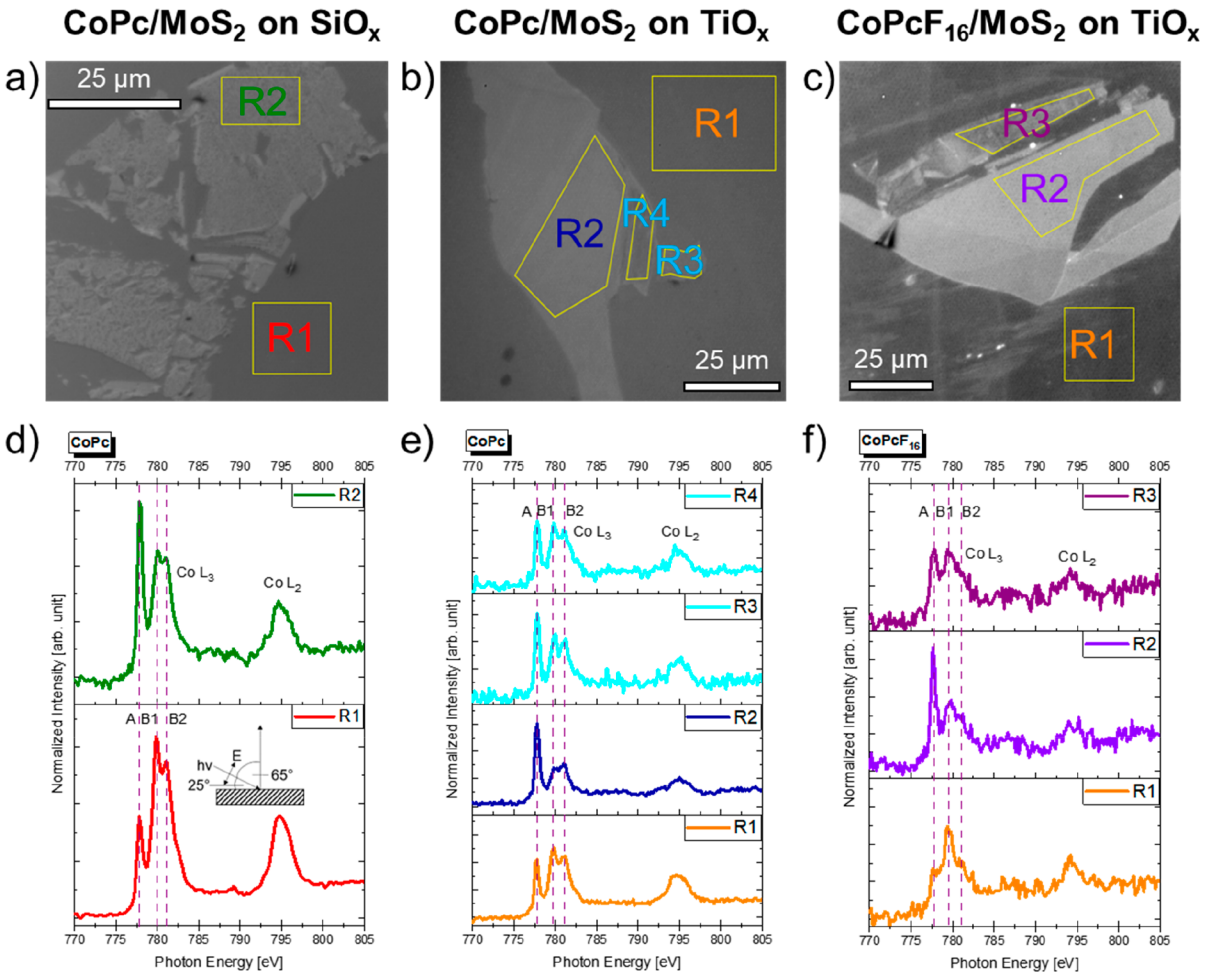

Figure 3. PEEM XAS measurements at an incident angle of 25° in the region of the Co L edge. (a–c) Average intensity images with an arbitrarily chosen grayscale to maximize contrast. Intensity differences are mostly based on secondary electron counts and, to a lesser extent, on spectral features. Selected regions of interests in these images are like those chosen for work function contrast measurements shown in Figure 2. (d–f) Normalized spectra of the respective RoI for the flakes 1–3 above.

dimensions of the MoS_2 flakes, a microscopic technique is needed. A certain PEEM measurement mode, spectromicroscopy, is particularly useful here. Spectromicroscopy essentially means taking stacks of PEEM images while scanning the incoming photon energy or the kinetic energy of the emitted electrons. By tracing a pixel (or lateral region) through the image stack, the former yields laterally resolved (μ-)XAS spectra, the latter laterally resolved (μ-)PES spectra. The resulting local spectra can be summed over regions of interest (RoIs) with freely defined shapes, as applied on measurements discussed in the following. In particular, microscopic measurements of the work function contrast have proven to be a very sensitive method for distinguishing monolayer and few-layer regions of TMDC flakes.[53−55]

In Figure 2, we show optical microscopy images, PEEM images, and corresponding μ-PES spectra of the secondary electron cutoff. In the following, we will refer to the flake on the oxidized silicon substrate (Figures 2a, d and S1) as flake 1, while the two flakes on the oxidized titanium substrates are referred to as flake 2 (Figures 2b, e, and S2) and flake 3 (Figures 2c, f and S3).

An initial indicator for estimating the number of layers can be provided by optical microscopy images. Differences in contrast between the substrate and the various layers in the flake (Figures 2a–c, S5, and S6) can be used to estimate the number of layers.[56,57] A detailed analysis of the red channel of optical microscope images (Figure S5) reveals a distinct difference between regions R3, which is assumed to be a single MoS_2 layer based on the photoluminescence,[58,59] and R4 in Figure 2e.

Furthermore, we will discuss the work function contrast of selected MoS_2 flakes prepared on naturally oxidized silicon and titanium substrates. Figure 2e–i shows PEEM images (the total diameter of the field of view is 126 μm for the measured circular images; the figures shown are cutouts, and the scales are adjusted accordingly) together with the normalized μ-PES spectra of the secondary electron cutoff. Generally, differences in the intensity of PEEM images are attributable to secondary electrons and, to a lesser extent, spectral features. Regions of interest (denoted R1 - R4 in Figure 2) were selected based on previously acquired optical microscope images and observable color variations (Figure 2a–c). Average spectra in Figure 2g–i were generated over all pixels in the chosen regions marked in Figure 2d–f. For a better comparison of the work functions, we measured the secondary electron cutoff from the pure substrates with a UPS at our laboratory spectrometer. We found a work function of 4.2 eV for the silicon and 3.6 eV for the titanium substrates, respectively (Figure S7g). This

difference is in good agreement with literature data and the relative differences we found in our PEEM measurements on the substrate regions (Figure S7d–f), marked R1 in each experiment. Therefore, we referenced the measured work functions of substrate region R1 to the values measured in the UPS experiments on the bare substrates. The energy scales of the MoS_2 flake regions are based on this calibration procedure.

We find almost the same work function for the pristine titanium substrate regions (R1) for the measurements containing flake 2 and flake 3, and a higher work function for the silicon substrate region containing flake 1. A comparably high work function Φ is expected for MoS_2; a value of 5.4 eV was recently reported for single-crystalline bulk substrates.[33] However, for monolayer or few-layers on oxidized silicon, significantly lower values were observed ($\Phi \sim 4.5$ eV) by both PEEM and Kelvin probe force microscopy (KPFM).[60,61] We note that KPFM measures relative work functions, which may complicate a direct comparison of the absolute values. Furthermore, a comparison to literature data has to take into account difference in the preparation method, the influence of contaminations in the case of measurements under ambient conditions,[60] as well as the choice of the substrate, which may alter the work function of MoS_2 flakes by several tenths of eV.[61] However, and most importantly, all methods agree in that the work function increases from single to few-layer MoS_2.[54,61,62] Using PEEM under UHV conditions, for MoS_2 on oxidized silicon, differences of 60 and 80 meV were observed from 1 to 2 and 2 to3 monolayers, respectively. Thus, the lower work function of regions R3 and R4 in Figure 2b, c clearly indicates a lower number of MoS_2 layers.

From these investigations, we estimate that flake 1 on the oxidized silicon substrate is a bilayer, region R3 of flake 2 on oxidized titanium is a monolayer, and region R4 is a trilayer. For region R3 of flake 3, we estimate it to consist of four layers. We note that this estimation is associated with a high degree of uncertainty. However, we were able to prepare samples that exhibit regions with a few layers of MoS_2, as well as thicker, bulk-like regions (R2 in Figure 2e and f).

In the next step, we deposited CoPc on the samples containing flakes 1 and 2, and $CoPcF_{16}$ on the sample containing flake 3 and measured PEEM-XAS in the Co $L_{3,2}$ region. According to the QCM data, the thickness was in the monolayer range. The corresponding PEEM images, together with the averaged Co $L_{3,2}$ edge spectra of the selected regions, are shown in Figure 3. The XAS spectra in Figure 3d–f were obtained by the analysis of PEEM images taken at different excitation energies. Generally, the XAS features discussed in Figure 1 are also visible in the μ-XAS spectra of Figure 3. Due to the fixed measurement geometry, all spectra were taken at an incident angle of 25° with respect to the surface of the sample. This is relatively close to the grazing incidence angle for the measurements of CoPc and $CoPcF_{16}$ on bulk MoS_2 single crystals (20°). Thus, for preferred predominantly flat-lying molecules only a slight increase in the relative intensity of the in-plane polarized features B1 and B2 might be expected compared to bulk MoS_2 single crystals, discussed in Figure 1 (cf., e.g., refs 34 and 48 for the angular dependence of Co L_3 spectra). A further reason for the slightly increased intensity of B1 and B2 could be a different degree of the polarization of the synchrotron light. Considering these minor technical limitations, the μ-XAS spectra of CoPc and $CoPcF_{16}$ on large MoS_2 terraces (R2) in Figure 3 are very similar to the related spectra on bulk MoS_2 single crystals at grazing incidence (20°) in Figure 1. In both cases, out-of-plane-polarized feature A clearly dominates the spectrum. In contrast, on the oxidized silicon and titanium surfaces (regions R1 in Figure 3), the molecules grow obviously in a different manner: The dominating in-plane features B1 and B2 indicate a preferred standing (edge-on) adsorption geometry, which can be related to the weaker molecule–substrate interaction with increasing (micro)roughness of the substrates (i.e., the substrates are not atomically flat). Such effects were reported for different molecules (see, e.g., refs 29 and 36). Most importantly, the ratio of A/B intensities of the Co L_3 spectra for regions R3 (flake 2 and flake 3) and R4 (flake 2) deviate distinctly from regions R2 of the MoS_2 flakes on oxidized titanium (Figure 3e and f), indicating significant tilt angles of the molecules to the surface plane or a disordered growth. This effect is observed to some weaker extent also in the region R2 on oxidized silicon (Figure 3d), where Figure 3a suggests a more inhomogeneous MoS_2 layer. The regions R3 (flake 2 and flake 3) and R4 (flake 2) are characterized by (i) a lower number of MoS_2 layers and (ii) by a smaller size compared to regions R2. Both could affect the molecular orientation of the deposited CoPc and $CoPcF_{16}$ molecules. The lower number of MoS_2 layers may affect the surface energy of the substrate, and the flexibility of the thin-layer MoS_2 may cause a certain corrugation due to the alignment at the substrate surface. The small lateral size of the thin MoS_2 regions might limit the favorable flat-lying adsorption geometry to a certain number of molecules and step-edge effects might become important. Another factor that can influence the surface energy, and consequently molecule–substrate interactions, particularly in mechanically exfoliated flakes of MoS_2, is defects.[63] Further investigation is needed to understand the different adsorption geometries of Co phthalocyanines on smaller MoS_2 terraces.

4. CONCLUSION

In conclusion, we found that the orientation of cobalt phthalocyanines on small-sized thin-layers of MoS_2 flakes is significantly different compared to that of bulk MoS_2. This demonstrates that the molecular orientation on small sized (mono- to few-layers) TMDC flakes cannot be simply deduced from the orientation of organic molecules on related bulk substrates. For the understanding of electronic and optic interactions at such interfaces, different molecular orientations should be considered. From our perspective, this could also affect TMDC-based devices as the situation between electrodes with small distances could lead to a similar restricted situation, in particular if the evaporation of molecules occurs after the deposition of electrode structures. In addition, defects in the flakes and the high cleanliness of in situ cleaned substrates might be important. Although our studies are focused on monolayer coverages, more extended growth studies varying the temperature, film thickness, and deposition rate are of high interest. Also, a systematic variation of the lateral size of atomically flat MoS_2 terraces may help to understand the observations discussed in this study. Thus, further research is needed to reveal the exact underlying mechanism for the different molecular orientations on bulk MoS_2 and flakes.

AUTHOR INFORMATION

Corresponding Authors

Heiko Peisert − *Institut für Physikalische und Theoretische Chemie, Universität Tübingen, 72076 Tübingen, Germany;* orcid.org/0000-0002-9742-5800; Phone: (+49) 07071/29-76931; Email: heiko.peisert@uni-tuebingen.de; Fax: (+49) 07071/29-5490

Marcus Scheele − *Institut für Physikalische und Theoretische Chemie, Universität Tübingen, 72076 Tübingen, Germany;* orcid.org/0000-0002-2704-3591; Email: marcus.scheele@uni-tuebingen.de

Authors

Philipp Haizmann − *Institut für Physikalische und Theoretische Chemie, Universität Tübingen, 72076 Tübingen, Germany*

Eric Juriatti − *Institut für Physikalische und Theoretische Chemie, Universität Tübingen, 72076 Tübingen, Germany*

Maren Klein − *Institut für Physikalische und Theoretische Chemie, Universität Tübingen, 72076 Tübingen, Germany*

Katharina Greulich − *Institut für Physikalische und Theoretische Chemie, Universität Tübingen, 72076 Tübingen, Germany*

Peter Nagel − *Institute for Quantum Materials and Technologies (IQMT), Karlsruhe Institute of Technology (KIT), 76021 Karlsruhe, Germany; Karlsruhe Nano and Micro Facility (KNMFi), Karlsruhe Institute of Technology, 76344 Eggenstein-Leopoldshafen, Germany*

Michael Merz − *Institute for Quantum Materials and Technologies (IQMT), Karlsruhe Institute of Technology (KIT), 76021 Karlsruhe, Germany; Karlsruhe Nano and Micro Facility (KNMFi), Karlsruhe Institute of Technology, 76344 Eggenstein-Leopoldshafen, Germany;* orcid.org/0000-0002-7346-7176

Stefan Schuppler − *Institute for Quantum Materials and Technologies (IQMT), Karlsruhe Institute of Technology (KIT), 76021 Karlsruhe, Germany; Karlsruhe Nano and Micro Facility (KNMFi), Karlsruhe Institute of Technology, 76344 Eggenstein-Leopoldshafen, Germany*

Amir Ghiami − *Institute for Quantum Materials and Technologies (IQMT), Karlsruhe Institute of Technology (KIT), 76021 Karlsruhe, Germany; Karlsruhe Nano and Micro Facility (KNMFi), Karlsruhe Institute of Technology, 76344 Eggenstein-Leopoldshafen, Germany*

Ruslan Ovsyannikov − *Institute for Methods and Instrumentation for Synchrotron Radiation Research, Helmholtz-Zentrum Berlin für Materialien und Energie GmbH, 12489 Berlin, Germany*

Erika Giangrisostomi − *Institute for Methods and Instrumentation for Synchrotron Radiation Research, Helmholtz-Zentrum Berlin für Materialien und Energie GmbH, 12489 Berlin, Germany*

Thomas Chassé − *Institut für Physikalische und Theoretische Chemie, Universität Tübingen, 72076 Tübingen, Germany;* orcid.org/0000-0001-6442-8944

Author Contributions

# P.H. and E.J. contributed equally.

Notes

The authors declare no competing financial interest.

ACKNOWLEDGMENTS

The authors thank the Helmholtz-Zentrum Berlin (electron storage ring BESSY II) for provision of synchrotron radiation at the beamline PM4. Financial travel support by HZB is thankfully acknowledged. The authors are grateful to the KIT Light Source, Karlsruhe, Germany, for the provision of beamtime. The Center for Light-Matter Interaction, Sensors & Analytics (LISA+) at the University of Tübingen is acknowledged for technical support and Fabian Strauß for the preparation of the substrates. The work was supported by the German Research Council (PE 546/17-1, SCHE1905/9-1 (project no. 426008387)) and the European Research Council (ERC) under the European Union's Horizon 2020 research and innovation program (Grant Agreement 802822).

REFERENCES

(1) Zeng, S. F.; Tang, Z. W.; Liu, C. S.; Zhou, P. Electronics based on two-dimensional materials: Status and outlook. *Nano Research* **2021**, *14* (6), 1752−1767.

(2) Fiori, G.; Bonaccorso, F.; Iannaccone, G.; Palacios, T.; Neumaier, D.; Seabaugh, A.; Banerjee, S. K.; Colombo, L. Electronics based on two-dimensional materials. *Nat. Nanotechnol.* **2014**, *9* (10), 768−779.

(3) Zheng, L.; Wang, X. W.; Jiang, H. J.; Xu, M. Z.; Huang, W.; Liu, Z. Recent progress of flexible electronics by 2D transition metal dichalcogenides. *Nano Research* **2022**, *15* (3), 2413−2432.

(4) Manzeli, S.; Ovchinnikov, D.; Pasquier, D.; Yazyev, O. V.; Kis, A. 2D transition metal dichalcogenides. *Nature Reviews Materials* **2017**, *2* (8), 17033.

(5) Novoselov, K. S.; Jiang, D.; Schedin, F.; Booth, T. J.; Khotkevich, V. V.; Morozov, S. V.; Geim, A. K. Two-dimensional atomic crystals. *Proc. Natl. Acad. Sci. U. S. A.* **2005**, *102* (30), 10451−10453.

(6) Wang, Q. H.; Kalantar-Zadeh, K.; Kis, A.; Coleman, J. N.; Strano, M. S. Electronics and optoelectronics of two-dimensional transition metal dichalcogenides. *Nat. Nanotechnol.* **2012**, *7* (11), 699−712.

(7) Radisavljevic, B.; Radenovic, A.; Brivio, J.; Giacometti, V.; Kis, A. Single-layer MoS2 transistors. *Nat. Nanotechnol.* **2011**, *6* (3), 147−150.

(8) Liu, Y.; Weiss, N. O.; Duan, X.; Cheng, H.-C.; Huang, Y.; Duan, X. Van der Waals heterostructures and devices. *Nature Reviews Materials* **2016**, *1* (9), 16042.

(9) Pham, P. V.; Bodepudi, S. C.; Shehzad, K.; Liu, Y.; Xu, Y.; Yu, B.; Duan, X. F. 2D Heterostructures for Ubiquitous Electronics and Optoelectronics: Principles, Opportunities, and Challenges. *Chem. Rev.* **2022**, *122* (6), 6514−6613.

(10) Nevola, D.; Hoffman, B. C.; Bataller, A.; Ade, H.; Gundogdu, K.; Dougherty, D. B. Rigid valence band shift due to molecular surface counter-doping of MoS2. *Surf. Sci.* **2019**, *679*, 254−258.

(11) Jing, Y.; Tan, X.; Zhou, Z.; Shen, P. W. Tuning electronic and optical properties of MoS2 monolayer via molecular charge transfer. *Journal of Materials Chemistry A* **2014**, *2* (40), 16892−16897.

(12) Park, S.; Schultz, T.; Xu, X. M.; Wegner, B.; Aljarb, A.; Han, A.; Li, L. J.; Tung, V. C.; Amsalem, P.; Koch, N. Demonstration of the

key substrate-dependent charge transfer mechanisms between monolayer MoS2 and molecular dopants. *Commun. Phys.* **2019**, *2*, 8.
(13) Huang, Y. L.; Zheng, Y. J.; Song, Z. B.; Chi, D. Z.; Wee, A. T. S.; Quek, S. Y. The organic-2D transition metal dichalcogenide heterointerface. *Chem. Soc. Rev.* **2018**, *47* (9), 3241−3264.
(14) Amsterdam, S. H.; Marks, T. J.; Hersam, M. C. Leveraging Molecular Properties to Tailor Mixed-Dimensional Heterostructures beyond Energy Level Alignment. *J. Phys. Chem. Lett.* **2021**, *12* (19), 4543−4557.
(15) Amsterdam, S. H.; Stanev, T. K.; Wang, L. Q.; Zhou, Q. F.; Irgen-Gioro, S.; Padgaonkar, S.; Murthy, A. A.; Sangwan, V. K.; Dravid, V. P.; Weiss, E. A.; et al. Mechanistic Investigation of Molybdenum Disulfide Defect Photoluminescence Quenching by Adsorbed Metallophthalocyanines. *J. Am. Chem. Soc.* **2021**, *143* (41), 17153−17161.
(16) Krumland, J.; Cocchi, C. Conditions for electronic hybridization between transition-metal dichalcogenide monolayers and physisorbed carbon-conjugated molecules. *Electronic Structure* **2021**, *3* (4), No. 044003.
(17) Casotto, A.; Drera, G.; Perilli, D.; Freddi, S.; Pagliara, S.; Zanotti, M.; Schio, L.; Verdini, A.; Floreano, L.; Di Valentin, C.; Sangaletti, L. pi-Orbital mediated charge transfer channels in a monolayer Gr-NiPc heterointerface unveiled by soft X-ray electron spectroscopies and DFT calculations. *Nanoscale* **2022**, *14* (36), 13166−13177.
(18) Koch, N. Opportunities for energy level tuning at inorganic/organic semiconductor interfaces. *Appl. Phys. Lett.* **2021**, *119* (26), 260501.
(19) Duhm, S.; Heimel, G.; Salzmann, I.; Glowatzki, H.; Johnson, R. L.; Vollmer, A.; Rabe, J. P.; Koch, N. Orientation-dependent ionization energies and interface dipoles in ordered molecular assemblies. *Nat. Mater.* **2008**, *7* (4), 326−332.
(20) Forrest, S. R. Ultrathin organic films grown by organic molecular beam deposition and related techniques. *Chem. Rev.* **1997**, *97* (6), 1793−1896.
(21) Kudo, K.; Wang, D. X.; Iizuka, M.; Kuniyoshi, S.; Tanaka, K. Schottky gate static induction transistor using copper phthalocyanine films. *Thin Solid Films* **1998**, *331* (1−2), 51−54.
(22) Bao, Z.; Lovinger, A. J.; Dodabalapur, A. Organic field-effect transistors with high mobility based on copper phthalocyanine. *Appl. Phys. Lett.* **1996**, *69* (20), 3066−3068.
(23) Melville, O. A.; Lessard, B. H.; Bender, T. P. Phthalocyanine-Based Organic Thin-Film Transistors: A Review of Recent Advances. *ACS Appl. Mater. Interfaces* **2015**, *7* (24), 13105−13118.
(24) Greulich, K.; Belser, A.; Basova, T.; Chasse, T.; Peisert, H. Interfaces between Different Iron Phthalocyanines and Au(111): Influence of the Fluorination on Structure and Interfacial Interactions. *J. Phys. Chem. C* **2022**, *126* (1), 716−727.
(25) Zhou, Q. F.; Liu, Z. F.; Marks, T. J.; Darancet, P. Electronic Structure of Metallophthalocyanines, MPc (M = Fe, Co, Ni, Cu, Zn, Mg) and Fluorinated MPc. *J. Phys. Chem. A* **2021**, *125* (19), 4055−4061.
(26) Toader, M.; Gopakumar, T. G.; Shukrynau, P.; Hietschold, M. Exploring the F16CoPc/Ag(110) Interface Using Scanning Tunneling Microscopy and Spectroscopy. 2. Adsorption-Induced Charge Transfer Effect. *J. Phys. Chem. C* **2010**, *114* (49), 21548−21554.
(27) Peisert, H.; Knupfer, M.; Schwieger, T.; Fuentes, G. G.; Olligs, D.; Fink, J.; Schmidt, T. Fluorination of copper phthalocyanines: Electronic structure and interface properties. *J. Appl. Phys.* **2003**, *93* (12), 9683−9692.
(28) Balle, D.; Adler, H.; Gruninger, P.; Karstens, R.; Ovsyannikov, R.; Giangrisostomi, E.; Chasse, T.; Peisert, H. Influence of the Fluorination of CoPc on the Interfacial Electronic Structure of the Coordinated Metal Ion. *J. Phys. Chem. C* **2017**, *121* (34), 18564−18574.
(29) Peisert, H.; Biswas, I.; Knupfer, M.; Chasse, T. Orientation and electronic properties of phthalocyanines on polycrystalline substrates. *Physica Status Solidi B-Basic Solid State Physics* **2009**, *246* (7), 1529−1545.
(30) Peisert, H.; Schwieger, T.; Auerhammer, J. M.; Knupfer, M.; Golden, M. S.; Fink, J.; Bressler, P. R.; Mast, M. Order on disorder: Copper phthalocyanine thin films on technical substrates. *J. Appl. Phys.* **2001**, *90* (1), 466−469.
(31) Kera, S.; Casu, M. B.; Bauchspiess, K. R.; Batchelor, D.; Schmidt, T.; Umbach, E. Growth mode and molecular orientation of phthalocyanine molecules on metal single crystal substrates: A NEXAFS and XPS study. *Surf. Sci.* **2006**, *600* (5), 1077−1084.
(32) Padgaonkar, S.; Amsterdam, S. H.; Bergeron, H.; Su, K.; Marks, T. J.; Hersam, M. C.; Weiss, E. A. Molecular-Orientation-Dependent Interfacial Charge Transfer in Phthalocyanine/MoS2Mixed-Dimensional Heterojunctions. *J. Phys. Chem. C* **2019**, *123* (21), 13337−13343.
(33) Greulich, K.; Belser, A.; Bölke, S.; Grüninger, P.; Karstens, R.; Sättele, M. S.; Ovsyannikov, R.; Giangrisostomi, E.; Basova, T. V.; Klyamer, D. D.; et al. Charge Transfer from Organic Molecules to Molybdenum Disulfide: Influence of the Fluorination of Iron Phthalocyanine. *J. Phys. Chem. C* **2020**, *124* (31), 16990−16999.
(34) Peisert, H.; Uihlein, J.; Petraki, F.; Chassé, T. Charge transfer between transition metal phthalocyanines and metal substrates: The role of the transition metal. *J. Electron Spectrosc. Relat. Phenom.* **2015**, *204*, 49−60.
(35) Scardamaglia, M.; Struzzi, C.; Lizzit, S.; Dalmiglio, M.; Lacovig, P.; Baraldi, A.; Mariani, C.; Betti, M. G. Energetics and Hierarchical Interactions of Metal Phthalocyanines Adsorbed on Graphene/Ir(111). *Langmuir* **2013**, *29* (33), 10440−10447.
(36) Breuer, T.; Salzmann, I.; Gotzen, J.; Oehzelt, M.; Morherr, A.; Koch, N.; Witte, G. Interrelation between Substrate Roughness and Thin-Film Structure of Functionalized Acenes on Graphite. *Cryst. Growth Des.* **2011**, *11* (11), 4996−5001.
(37) Schmidt, T.; Wilkens, T.; Falta, J. Ordering of copper phthalocyanine films on functionalized Si(111). *Surf. Sci.* **2022**, *725*, 122127.
(38) Cranston, R. R.; Lessard, B. H. Metal phthalocyanines: thin-film formation, microstructure, and physical properties. *RSC Adv.* **2021**, *11* (35), 21716−21737.
(39) Evans, D. A.; Steiner, H. J.; Vearey-Roberts, A. R.; Bushell, A.; Cabailh, G.; O'Brien, S.; Wells, J. W.; McGovern, I. T.; Dhanak, V. R.; Kampen, T. U.; et al. Synchrotron radiation studies of inorganic-organic semiconductor interfaces. *Nuclear Instruments & Methods in Physics Research Section B-Beam Interactions with Materials and Atoms* **2003**, *199*, 475−480.
(40) Ballirano, P.; Caminiti, R.; Ercolani, C.; Maras, A.; Orrù, M. A. X-ray Powder Diffraction Structure Reinvestigation of the α and β Forms of Cobalt Phthalocyanine and Kinetics of the $\alpha \rightarrow \beta$ Phase Transition. *J. Am. Chem. Soc.* **1998**, *120* (49), 12798−12807.
(41) de Oteyza, D. G.; Barrena, E.; Zhang, Y.; Krauss, T. N.; Turak, A.; Vorobiev, A.; Dosch, H. Experimental Relation between Stranski−Krastanov Growth of DIP/F16CoPc Heterostructures and the Reconstruction of the Organic Interface. *J. Phys. Chem. C* **2009**, *113* (11), 4234−4239.
(42) Giangrisostomi, E.; Ovsyannikov, R.; Sorgenfrei, F.; Zhang, T.; Lindblad, A.; Sassa, Y.; Cappel, U. B.; Leitner, T.; Mitzner, R.; Svensson, S.; et al. Low Dose Photoelectron Spectroscopy at BESSY II: Electronic structure of matter in its native state. *J. Electron Spectrosc. Relat. Phenom.* **2018**, *224*, 68−78.
(43) Novoselov, K. S.; Castro Neto, A. H. Two-dimensional crystals-based heterostructures: materials with tailored properties. *Phys. Scr.* **2012**, *T146* (T146), No. 014006.
(44) Schneider, C. A.; Rasband, W. S.; Eliceiri, K. W. NIH Image to ImageJ: 25 years of image analysis. *Nat. Methods* **2012**, *9* (7), 671−675.
(45) Schindelin, J.; Arganda-Carreras, I.; Frise, E.; Kaynig, V.; Longair, M.; Pietzsch, T.; Preibisch, S.; Rueden, C.; Saalfeld, S.; Schmid, B.; et al. Fiji: an open-source platform for biological-image analysis. *Nat. Methods* **2012**, *9* (7), 676−682.
(46) Stöhr, J. *NEXAFS Spectroscopy*; Springer, 1992.
(47) Stöhr, J.; Outka, D. A. Determination of molecular orientations on surfaces from the angular dependence of near-edge x-ray-

absorption fine-structure spectra. *Phys. Rev. B* **1987**, *36* (15), 7891−7905.
(48) Kroll, T.; Aristov, V. Y.; Molodtsova, O. V.; Ossipyan, Y. A.; Vyalikh, D. V.; Büchner, B.; Knupfer, M. Spin and orbital ground state of Co in cobalt phthalocyanine. *J. Phys. Chem. A* **2009**, *113* (31), 8917−8922.
(49) de Groot, F. Multiplet effects in X-ray spectroscopy. *Coord. Chem. Rev.* **2005**, *249* (1−2), 31−63.
(50) Zhang, T.; Brumboiu, I. E.; Lanzilotto, V.; Luder, J.; Grazioli, C.; Giangrisostomi, E.; Ovsyannikov, R.; Sass, Y.; Bidermane, I.; Stupar, M.; et al. Conclusively Addressing the CoPc Electronic Structure: A Joint Gas-Phase and Solid-State Photoemission and Absorption Spectroscopy Study. *J. Phys. Chem. C* **2017**, *121* (47), 26372−26378.
(51) Brumboiu, I. E.; Haldar, S.; Luder, J.; Eriksson, O.; Herper, H. C.; Brena, B.; Sanyal, B. Influence of Electron Correlation on the Electronic Structure and Magnetism of Transition-Metal Phthalocyanines. *J. Chem. Theory Comput.* **2016**, *12* (4), 1772−1785.
(52) Belser, A.; Greulich, K.; Grüninger, P.; Karstens, R.; Ovsyannikov, R.; Giangrisostomi, E.; Nagel, P.; Merz, M.; Schuppler, S.; Chassé, T.; Peisert, H. Perfluorinated Phthalocyanines on Cu(110) and Cu(110)-(2 × 1)O: The Special Role of the Central Cobalt Atom. *J. Phys. Chem. C* **2021**, *125* (16), 8803−8814.
(53) Keyshar, K.; Berg, M.; Zhang, X.; Vajtai, R.; Gupta, G.; Chan, C. K.; Beechem, T. E.; Ajayan, P. M.; Mohite, A. D.; Ohta, T. Experimental Determination of the Ionization Energies of MoSe2, WS2, and MoS2 on SiO2 Using Photoemission Electron Microscopy. *ACS Nano* **2017**, *11* (8), 8223−8230.
(54) Berg, M.; Keyshar, K.; Bilgin, I.; Liu, F. Z.; Yamaguchi, H.; Vajtai, R.; Chan, C.; Gupta, G.; Kar, S.; Ajayan, P. Layer dependence of the electronic band alignment of few-layer MoS2 on SiO2 measured using photoemission electron microscopy. *Phys. Rev. B* **2017**, *95* (23), 235406.
(55) Fregnaux, M.; Kim, H.; Rouchon, D.; Derycke, V.; Bleuse, J.; Voiry, D.; Chhowalla, M.; Renault, O. Chemistry and electronics of single layer MoS2 domains from photoelectron spectromicroscopy using laboratory excitation sources. *Surf. Interface Anal.* **2016**, *48* (7), 465−469.
(56) Li, H.; Wu, J.; Huang, X.; Lu, G.; Yang, J.; Lu, X.; Xiong, Q.; Zhang, H. Rapid and Reliable Thickness Identification of Two-Dimensional Nanosheets Using Optical Microscopy. *ACS Nano* **2013**, *7* (11), 10344−10353.
(57) Late, D. J.; Liu, B.; Matte, H. S. S. R.; Rao, C. N. R.; Dravid, V. P. Rapid Characterization of Ultrathin Layers of Chalcogenides on SiO2/Si Substrates. *Adv. Funct. Mater.* **2012**, *22* (9), 1894−1905.
(58) Golovynskyi, S.; Irfan, I.; Bosi, M.; Seravalli, L.; Datsenko, O. I.; Golovynska, I.; Li, B.; Lin, D.; Qu, J. Exciton and trion in few-layer MoS2: Thickness- and temperature-dependent photoluminescence. *Appl. Surf. Sci.* **2020**, *515*, 146033.
(59) Splendiani, A.; Sun, L.; Zhang, Y.; Li, T.; Kim, J.; Chim, C. Y.; Galli, G.; Wang, F. Emerging photoluminescence in monolayer MoS2. *Nano Lett.* **2010**, *10* (4), 1271−1275.
(60) Ochedowski, O.; Marinov, K.; Scheuschner, N.; Poloczek, A.; Bussmann, B. K.; Maultzsch, J.; Schleberger, M. Effect of contaminations and surface preparation on the work function of single layer MoS2. *Beilstein Journal of Nanotechnology* **2014**, *5*, 291−297.
(61) Lattyak, C.; Gehrke, K.; Vehse, M. Layer-Thickness-Dependent Work Function of MoS2 on Metal and Metal Oxide Substrates. *J. Phys. Chem. C* **2022**, *126* (32), 13929−13935.
(62) Tamulewicz, M.; Kutrowska-Girzycka, J.; Gajewski, K.; Serafinczuk, J.; Sierakowski, A.; Jadczak, J.; Bryja, L.; Gotszalk, T. P. Layer number dependence of the work function and optical properties of single and few layers MoS2: effect of substrate. *Nanotechnology* **2019**, *30* (24), 245708.
(63) Liang, Y.; Li, B.-H.; Li, Z.; Zhang, G.; Sun, J.; Zhou, C.; Tao, Y.; Ye, Y.; Ren, Z.; Yang, X. Spatially heterogeneous ultrafast interfacial carrier dynamics of 2D-MoS2 flakes. *Materials Today Physics* **2021**, *21*, 100506.